



*Citation for published version:*

Mashao, DC, Kosch, MJ, Füllekrug, M & Mlynarczyk, J 2022, 'Lightning parameters of sprites and diameter of halos over South Africa', *Journal of Atmospheric and Solar-Terrestrial Physics*, vol. 240, 105957.  
<https://doi.org/10.1016/j.jastp.2022.105957>

*DOI:*

[10.1016/j.jastp.2022.105957](https://doi.org/10.1016/j.jastp.2022.105957)

*Publication date:*

2022

*Document Version*

Peer reviewed version

[Link to publication](#)

*Publisher Rights*

CC BY-NC-ND

**University of Bath**

**Alternative formats**

If you require this document in an alternative format, please contact:  
[openaccess@bath.ac.uk](mailto:openaccess@bath.ac.uk)

**General rights**

Copyright and moral rights for the publications made accessible in the public portal are retained by the authors and/or other copyright owners and it is a condition of accessing publications that users recognise and abide by the legal requirements associated with these rights.

**Take down policy**

If you believe that this document breaches copyright please contact us providing details, and we will remove access to the work immediately and investigate your claim.

# 1 **Lightning parameters of sprites and diameter of halos**

2 **D.C Mashao<sup>1,2</sup>, M.J Kosch<sup>2,3,4</sup>, M. Füllekrug<sup>5</sup>, and J. Mlynarczyk<sup>6</sup>**

3 <sup>1</sup>Department of Physics, University of KwaZulu-Natal, Durban, South Africa

4 <sup>2</sup>South African National Space Agency, Hermanus, South Africa

5 <sup>3</sup>Department of Physics, Lancaster University, UK

6 <sup>4</sup>Department of Physics, University of Western Cape, Bellville, South Africa

7 <sup>5</sup>Department of Electronic and Electrical Engineering, University of Bath, Bath, UK

8 <sup>6</sup>Institute of Electronics, AGH University of Science and Technology, Krakow, Poland

9 **Corresponding author:** Dakalo Mashao (mashaodakalo@gmail.com)

## 10 **Abstract**

11 Transient Luminous Events (TLEs) above thunderclouds have been associated with variables  
12 such as the lightning Charge Moment Change (CMC), charge height, charge transfer, and  
13 rise-time. We show for the first time a survey of the CMC, rise-time, fall-time, peak electric  
14 field, and peak current of the lightning discharges associated with 11 column, 11 carrot, and  
15 18 sprites with halo. We found that carrot sprites are induced by a lightning discharge with  
16 CMC, peak electric field, and peak current greater and less than that for column sprites and  
17 sprites with halo, respectively. Sprites with a halo are initiated by a lightning discharge with a  
18 longer rise-time and fall-time than that for column and carrot sprites. Column sprites top  
19 altitude and carrot sprites brightest region altitude positively correlate with lightning rise-  
20 time. Lightning fall-time, peak electric field, and peak current increase with a decrease in the  
21 top and brightest region altitudes for carrot sprites. For the altitude of the sprites brightest  
22 region, column sprites correlate negatively with lightning fall-time, peak electric field, and  
23 CMC, and column sprites top altitude also correlates negatively with lightning peak electric  
24 field. Sprites with a halo top altitude increased with lightning fall-time and peak current, and  
25 sprites with a halo brightest altitude increased with an increase in lightning CMC. Halo  
26 diameters correlate positively with lightning fall-time, peak electric field, and peak current.

27 **Keywords:** Lightning rise-time; lightning fall-time; lightning Charge Moment Change;  
28 Lightning electric field; Lightning current; Transient Luminous Events altitude

29

## 30 1. Introduction

31 Sprites are vertically oriented luminous electric discharges induced by the cloud-to-ground  
32 (CG) lightning quasi-static electric field and continuing current. They appear at stratospheric  
33 and mesospheric altitudes of about 40 to 100 km (Füllekrug et al., 2006; Liu et al., 2015;  
34 Pasko, 2010; Pasko et al., 2013; Siingh et al., 2012; Surkov and Hayakawa, 2020). In  
35 contrast, halos manifest as a horizontal disc of luminous emission, also generated by the CG  
36 lightning quasi-static electric field and continuing current, at ionospheric altitudes of about 85  
37 km. The duration of the electric field at a certain altitude is almost equivalent to the local  
38 Maxwellian relaxation time, which is defined as the permittivity of free space over the local  
39 conductivity. The local Maxwellian relaxation time increases with a decrease in atmospheric  
40 altitude (Liu et al., 2015; Pasko et al., 1997).

41 Sprites and halos may be induced by mainly positive CG lightning electric fields, although  
42 some are generated by negative CG lightning discharge. Sprite streamers tend to develop  
43 from halos (Luque & Ebert, 2009). Column sprites are associated with only the downwards  
44 propagation of streamers, whereas carrot sprites are associated with both downwards and  
45 upwards streamer propagation (Bór, 2013). The Transient Luminous Events (TLE) manifest  
46 themselves about 1—100 ms after the parent CG lightning flash. (Bering et al., 2004; Chen et  
47 al., 2019; Frey et al., 2007; Liu et al., 2015; McHarg et al., 2002; Siingh et al., 2012;  
48 Williams et al., 2012). The parent lightning waveforms are shorter than the duration of the  
49 TLE luminosity.

50 Parameters such as lightning charge height, charge transfer, rise-time, and Charge Moment  
51 Change (CMC) are essential in determining whether the lightning stroke initiates sprites or  
52 halos (Asano et al., 2008; Yaniv et al., 2014; Haspel et al., 2020; Li et al., 2008; Mashao et  
53 al., 2021). Lightning with a mean and minimum CMC value of approximately 1480 C-km  
54 and 63 C-km has been associated with the generation of sprites (Chen et al., 2019).

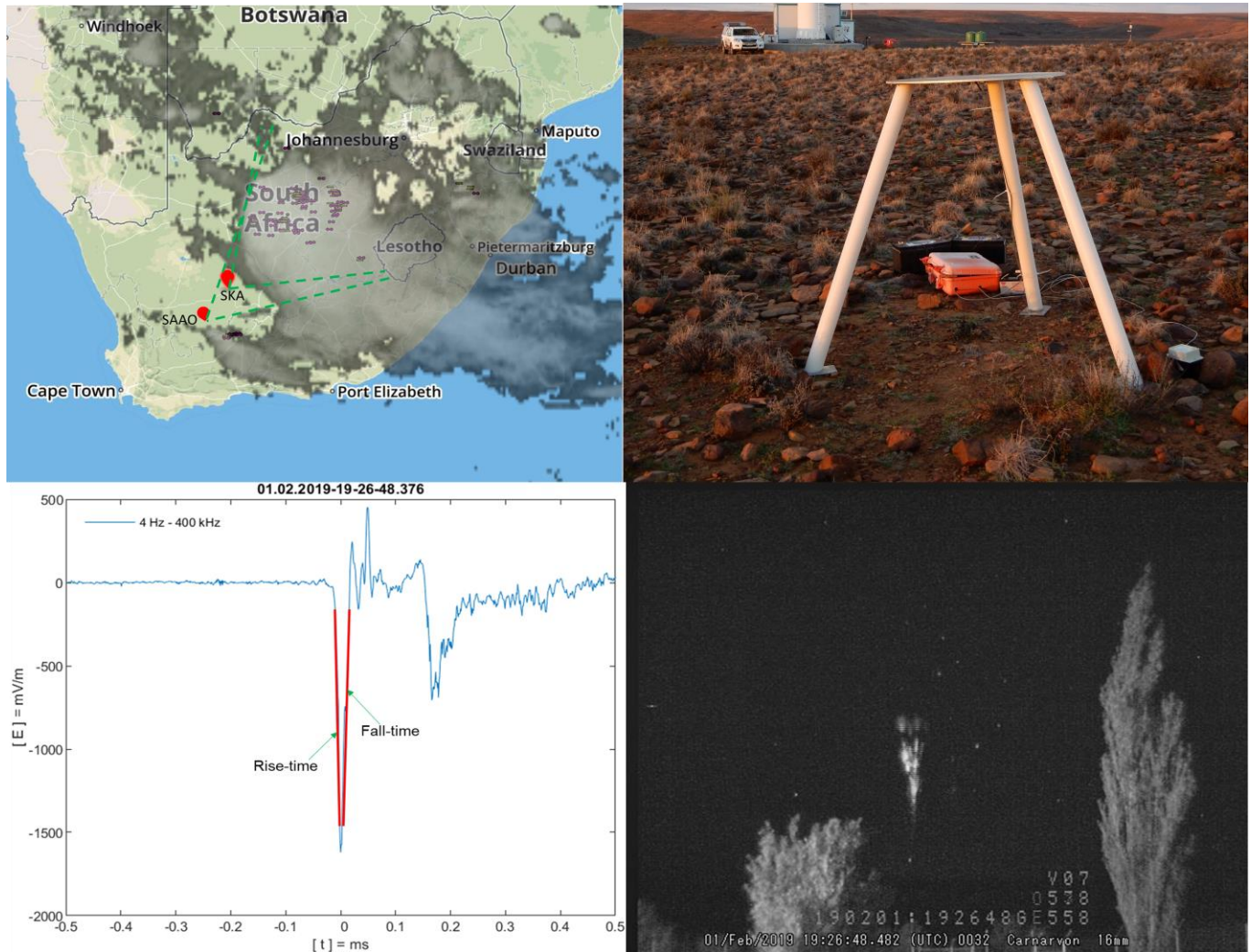
55 Enhancement in sprites brightness with an increase in lightning CMC has been reported by  
56 Yaniv et al. (2014), Yang et al. (2017), and Nnadih et al. (2018). Mashao et al. (2021)  
57 demonstrated a positive correlation between lightning CMC and sprites top altitude. The  
58 importance of lightning rise-time on sprites has been established by Asano et al. (2008) using  
59 a two-dimensional computer simulation for summer and winter storm conditions. According  
60 to Asano et al. (2008), lightning charge height, charge transfer, and rise-time are essential in  
61 the generation and development of sprites. The sprites breakdown region reduces in altitude

62 for a longer rise-time ( $>25 \mu\text{s}$ ) (Asano et al., 2008). We are not aware of any reported  
63 lightning fall-time regarding TLEs.

64 The altitudes of sprites have been well established using different techniques and high-speed  
65 cameras. The sprites top altitude has been observed to vary from 73 to 96 km, whereas the  
66 altitude of the sprites brightest region has been found to span from 50 to 84.1 km (Füllekrug  
67 et al., 2019; Luque et al., 2016; Mashao et al., 2021 Malagón-Romero et al., 2020; Sentman  
68 et al., 1995; Stenbaek-Nielsen et al., 2010; Wescott et al., 1998). Mashao et al. (2021) found  
69 that the average sprites top altitude in South Africa occurred at approximately 84.3 km. Other  
70 authors found sprite top altitudes at 88 km (Sentman et al., 1995), 86.4 km (Wescott et al.,  
71 1998), and 79-96 km (Stenbaek-Nielsen et al., 2010). Mashao et al. (2021) found that the  
72 average altitude of maximum brightness in South Africa occurred at approximately 69 km.  
73 Other authors found the altitude of maximum brightness at 70 km (Malagon-Romero et al.,  
74 2020) and 71.2-72.4 km (Luque et al., 2016). Wescott et al. (2001) observed that the top  
75 altitude of sprites with halos varied from 73.5 km to 85.2 km, with an apparent diameter of  
76 about 66 km. Taylor et al. (2008) found a diameter of about  $89 \pm 5$  km for a negative CG  
77 sprite with a halo. According to Miyasato et al. (2002), the average halo diameter was about  
78 86 km.

79 In this paper, we demonstrate for the first time the importance of lightning CMC, peak  
80 electric field, peak current, rise-time, and fall-time on sprites altitude and halo diameters for  
81 different sprites morphologies. This is done by evaluating the linear correlation between  
82 lightning CMC, peak electric field, peak current, rise-time, and fall-time versus the top  
83 altitude and altitude of the brightest region of column sprites, carrot sprites, and any sprites  
84 with halos. In addition, we measure the diameter of halos in South Africa for the first time.

## 85 2. Observations



86

87 Fig. 1. South African map (top left panel, obtained from EarthNetworks) denoting the thunderstorm which  
 88 initiated some of the TLEs in this paper and observation sites (red dots) of the South African Astronomical  
 89 Observatory (SAAO) and Square Kilometre Array (SKA) in the Northern Cape, South Africa. The green dotted  
 90 lines show camera viewing directions. The yellow plus, yellow negative, and pink dash-like symbols denote the  
 91 positive CG, negative CG, and intracloud lightning, respectively. Lightning vertical electric field (bottom left  
 92 panel) associated with a carrot sprite (bottom right panel) measured by the ELF receiver (4 Hz- 400 kHz) (top  
 93 right panel). The red lines (bottom left panel) indicate where the rise-time and fall-time were calculated from  
 94 90% to 10% of the maximum electric field signal deflection from the background. A carrot sprite recorded on 01  
 95 February 2019 at 19:26:48.558 UTC (bottom right panel) using a Watec 910Hx camera.

### 96 2.1 Camera systems

97 The 2019 sprites campaign was conducted from 28 January to 15 February 2019. Out of  
 98 about 208 TLEs, 40 TLEs consisting of 11 column, 11 carrot, and 18 sprites with halos were  
 99 selected for our analysis. The TLEs presented here were recorded using Watec 910Hx  
 100 cameras (Bór, 2013; Gamerota et al., 2011; Liu et al., 2016; Soula et al., 2009; Stenbaek-

101 Nielsen et al., 2010; Yaniv et al., 2014). We selected the TLEs that only contain column,  
102 carrot, and sprites with a halo to make a fair parent lightning parameters comparison.  
103 However, sprites with a halo consist of column, carrot, wishbone, and jellyfish sprites. Fig. 1  
104 (top left panel) shows two distinct locations; the Square Kilometre Array (SKA) ( $30.97^\circ$  S,  
105  $21.98^\circ$  E) and the South African Astronomical Observatory (SAAO) ( $32.38^\circ$  S,  $20.81^\circ$  E),  
106 where the Watec 910Hx cameras were operated. Both locations are in the Karroo desert of  
107 the Northern Cape of South Africa, see Fig. 1 (top left panel). Several Mesoscale Convection  
108 Systems (MCS) initiated the TLEs, moving from the northwest to the southeast over South  
109 Africa on 29 and 30 January as well as 1, 2, and 11 February 2019. The MCS produce TLEs  
110 for about 4 hours on average each night. Fig. 1 (top left panel) shows one MCS that induced  
111 the observed TLEs events (<https://www.earthnetworks.com/product/decision-support-collaboration-tools/sferic-maps/>). The 40 TLEs presented here were recorded on 29, 30  
113 January and 11 February 2019 from SAAO and 1 and 2 February 2019 from SKA. Fig. 1  
114 (bottom right panel) shows an example carrot sprite observed from SKA on 1 February 2019.  
115 The Watec 910Hx cameras had a 8.0 mm f/1.4 C-mount lens, giving a field of view (FOV) of  
116  $46.2^\circ$  horizontal and  $29^\circ$  vertical. The Watec 910Hx cameras operated under fixed gain and a  
117 gamma factor of 0.45. The observation systems recorded sprites video clips at 25 fps with a  
118 40 ms frame period. A GPS video timer installed in one camera system provided millisecond  
119 timing. A Network Timing Protocol server provided timing accuracy of about 1 ms for the  
120 other camera systems at SKA and SAAO. The camera systems operated with 8-bit intensity  
121 resolution. The video images had a size of 640x480 pixels with an angular resolution of  
122  $0.072^\circ$  horizontal and  $0.061^\circ$  vertical per pixel. Thus, 1 pixel is  $0.061^\circ$  in elevation angle.

## 123 **2.2 Altitude estimation**

124 The stars in the sprites image background allowed us to determine the azimuth and elevation  
125 angle of every pixel. The stars declination and right ascension from the star almanac, event  
126 time, and observation site were used to fit the modeled stars onto the real stars in the sprites  
127 image background in order to find the camera pointing direction and FOV, and to determine  
128 the azimuth and elevation angle of each pixel. To estimate the altitude of sprites, we assumed  
129 that sprites were induced directly above their parent CG lightning strokes. This supposition is  
130 usually used in TLEs studies (Füllekrug et al., 2019; Li et al., 2008; Luque et al., 2016;  
131 Mashao et al., 2021; McHarg et al., 2007). The sprites altitude was estimated from their  
132 elevation angle and ground distance from the observation location. This was done by  
133 employing planar trigonometry in the vertical plane and spherical trigonometry in the

134 horizontal plane. The method is fully described in Mashao et al. (2021). The altitude of  
135 sprites uncertainty, which depends on the slant distance between observation location and  
136 targeted sprites altitude, spanned  $\pm 0.33$ - $0.47$  km.

137 The sprites altitudes were estimated for two regions: the top altitude and the altitude of the  
138 brightest region. For a vertical profile through each TLE, the top altitude is the highest  
139 elevation angle pixel with an intensity value greater than the background. The diameter of the  
140 halos is determined in the same way for a horizontal profile. The altitude of maximum  
141 brightest is taken from the pixel of greatest intensity value within the TLE. The sprite top  
142 altitude is where electric field energy within a sprite is normally less than the altitude  
143 dependent critical breakdown field. The brightest region is where photon production  
144 maximizes due to collisions between the accelerated electrons and background neutrals (Liu  
145 et al., 2015; Mashao et al., 2021).

### 146 **2.3 Lightning detection**

147 We obtained the lightning information (time, position, peak current) of the TLEs parent CG  
148 lightning strokes from the South African Weather Service (SAWS) and Earth Networks (EN)  
149 (Gijben, 2012; Zhu et al., 2017). The parent CG lightning strokes were located between 242  
150 and 707.5 km away from the observation sites, so well within the maximum observing range  
151 (900 km). The parent lightning strokes were all of the positive polarity with a peak current  
152 spanning from 32 to 179 kA. Based on timing data, SAWS and EN did not detect all  
153 lightning discharges which initiated the TLEs. This limited the number of TLEs to report.

### 154 **2.4 Electromagnetic Waveforms**

155 A wideband digital ELF radio receiver, co-located with the cameras, detected the lightning  
156 vertical electric field strength associated with the optical sprites in the frequency ranging  
157 from  $\sim 4$  Hz to  $\sim 400$  kHz with a sampling frequency of 1 MHz and timing accuracy of 12 ns  
158 (see Fig. 1, top right panel) (Füllekrug, 2010). The ELF radio receiver was positioned in a  
159 low radio interference area near the SKA site. The TLEs parent lightning electric field  
160 strength span 1.0-3.8 V/m at the ELF radio receiver location. The lightning rise-time and fall-  
161 time were computed from the vertical electric field measured simultaneously with the optical  
162 observations (Füllekrug, 2010; Füllekrug et al., 2019). The rise-time calculations were from  
163 90% to 10% of the maximum electric field signal deflection from background. The same  
164 method was applied to the fall-time (see Fig. 1, bottom left panel).

165 The lightning CMC values ranged from 689 to 6,780 C-km and were computed from the far-  
166 field magnetic field data recorded by a broadband ELF system installed in the Bieszczady  
167 mountains in Poland (49.20° N, 22.54° E), using the method described by Mlynarczyk et al.  
168 (2015). The ELF system measures the two horizontal magnetic field components in the  
169 frequency range from 0.01 to 1,000 Hz with a sampling frequency of 3 kHz (Mlynarczyk et  
170 al., 2018). Due to signal noise and unknown locations of the parent lightning strokes, we  
171 could compute the lightning CMC for 31 TLEs, see Table 1 in the appendix.

172 All data are summarized in Table 1 in the appendix.

### 173 **3. Results and discussions**

174 An analysis of lightning rise-time, fall-time, peak electric field, peak current, and CMC  
175 associated with TLEs was conducted on 11 column sprites, 11 carrot sprites, and 18 any  
176 sprites with halos. Note that the sprites with halos have different morphologies, i.e., column,  
177 carrot, wishbone, and jellyfish. The lightning electric radiated fields propagate as  $1/r^2$ ,  
178 where  $r$  is the distance from the lightning location to the receiver location (Cooray and  
179 Lobato, 2020). For comparison, we normalized the lightning peak electric field values for the  
180 distance from the ELF receiver to the lightning stroke location. This was done by multiplying  
181 the lightning peak electric field values by the distance squared (in km) relative to 1 km  
182 (Taylor and Jean, 1959).

183 The lightning normalized peak electric field, peak current, rise-time, fall-time, and CMC  
184 associated with the analyzed TLEs vary from 93 to 914 kV/m, 32 to 179 kA, 6 to 25  $\mu$ s, 1 to  
185 91  $\mu$ s, and 689 to 6,780 C-km, respectively. Most of the investigated TLEs producing parent  
186 lightning had a very short rise-time ( $<15 \mu$ s) and short fall-time ( $<25 \mu$ s); see Table 1. We  
187 found that TLEs top altitudes vary from 71 to 90.5 km, with an average and standard  
188 deviation of 79.8 and 5.2 km, respectively. The TLEs top altitudes are in the altitude range  
189 previously reported in the literature (Füllekrug et al., 2019; Luque et al., 2016; Mashao et al.,  
190 2021 Malagón-Romero et al., 2020; Sentman et al., 1995; Stenbaek-Nielsen et al., 2010;  
191 Wescott et al., 1998). The analyzed TLEs brightest region altitude ranged from 50 to 73 km,  
192 with an average and standard deviation of 61.5 and 6.4 km, respectively. The TLEs altitude  
193 of maximum brightness are in the altitude range reported in the literature (Füllekrug et al.,  
194 2019; Luque et al., 2016; Mashao et al., 2021 Malagón-Romero et al., 2020; Sentman et  
195 al., 1995; Stenbaek-Nielsen et al., 2010; Wescott et al., 1998).



196 The top altitude for column sprites, carrot sprites, and sprites with halos (halo top) varied  
197 from 72.4 to 86.4 km, 70.7 to 87 km, and 71.5 to 90.5 km, respectively. We obtained an  
198 average top altitude for column sprites, carrot sprites, and sprites with halos of about 80.4,  
199 80.6, and 78.9 km, with the standard deviation of about 4.6, 5.1, and 5.6 km, respectively.  
200 The brightest region altitude for column sprites, carrot sprites, and sprites with halos ranged  
201 from 55.1 to 73 km, 50 to 68.5 km, and 50 to 68 km, respectively. The average altitude for  
202 column, carrot, and sprites with halos was 66 (6.5), 61 (5.5), and 59 (5.2) km, where the  
203 value in parenthesis is the standard deviation.

204 The lightning peak electric field, peak current, CMC, rise-time, and fall-time for column  
205 sprites ranged from 101 to 355 kV/m, 34 to 87 kA, 880 to 2,410 C-km, 7 to 16  $\mu$ s, and 1 to 30  
206  $\mu$ s, respectively, with an average of 211 (74) kV/m, 48.5 (15.2) kA, 1,674 (583) C-km, 11.1  
207 (2.8)  $\mu$ s, and 15.3 (8.1)  $\mu$ s, where the value in parentheses is the standard deviation. Carrot  
208 sprites were induced by lightning flashes with peak electric field, peak current, CMC, rise-  
209 time, and fall-time varying from 93 to 427 kV/m, 32 to 92 kA, 1,360 to 3,060 C-km, 6 to 19  
210  $\mu$ s, and 1 to 32  $\mu$ s, respectively, with an average of 233 (125) kV/m, 58 (17.4) kA, 2,187  
211 (601) C-km, 11 (5)  $\mu$ s, and 15.6 (12.2)  $\mu$ s. The lightning peak electric field, peak current,  
212 CMC, rise-time, and fall-time, which initiated any sprites with halos, had values ranging from  
213 180 to 914 kV/m, 60 to 179 kA, 639 to 6,780 C-km, 8 to 25  $\mu$ s, and from 10 to 91  $\mu$ s,  
214 respectively, with an average of 519 (210) kV/m, 106.2 (30.6) kA, 2,909 (1,983) C-km, 12.8  
215 (4.8)  $\mu$ s, and 36.3 (22.4)  $\mu$ s.

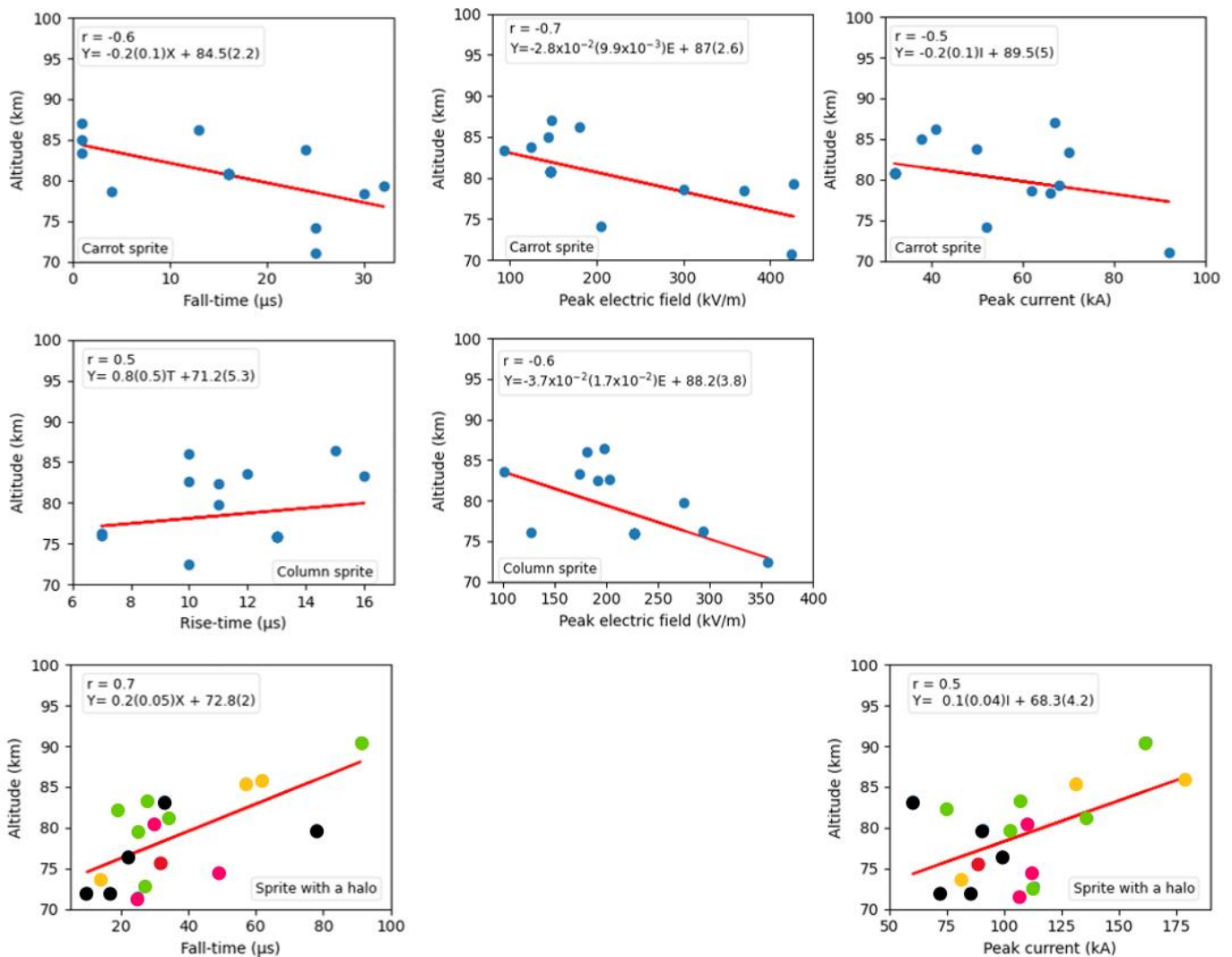
216 Clearly, column and carrot sprites require a less lightning CMC and smaller lightning rise-  
217 time and fall-time compared to any sprites with a halo. Sprites with halos require a  
218 significantly greater lightning CMC and significantly longer lightning fall-time when  
219 compared to carrot and column sprites, as shown in Table 1. Column sprites require a lower  
220 lightning electric field and peak current compared to carrot sprites and sprites with a halo.  
221 The lightning discharges which initiate carrot sprites have a CMC, peak electric field, and  
222 peak current greater and less than that of the column sprites and sprites with halo,  
223 respectively.

224 We correlated the various lightning parameters against the brightest region and top altitude of  
225 column, carrot, and sprites with halo, and their relationships are presented below. According  
226 to Peat et al. (2009), Pearson's linear correlation coefficients spanning from 0.1 to 0.3 are  
227 small correlations, 0.3 to 0.5 are moderate correlations, and greater than 0.5 are high  
228 correlations.

### 229 3.1 Sprites top altitude

230 Fig. 2 shows the relationship between lightning fall-time ( $X$ ,  $\mu\text{s}$ ) (top left row), normalized  
 231 peak electric field ( $E$ ,  $\text{kV/m}$ ) (top middle row), and peak current ( $I$ ,  $\text{kA}$ ) (top right row) versus  
 232 the top altitude ( $Y$ ,  $\text{km}$ ) of carrot sprites. Fig. 2 also shows lightning rise-time ( $T$ ,  $\mu\text{s}$ ) (middle  
 233 left row) and normalized peak electric field ( $E$ ,  $\text{kV/m}$ ) (middle center row) versus the top  
 234 altitude ( $Y$ ,  $\text{km}$ ) of column sprites, as well as lightning fall-time ( $X$ ,  $\mu\text{s}$ ) (bottom left row) and  
 235 peak current ( $I$ ,  $\text{kA}$ ) (bottom right row) versus top altitude ( $Y$ ,  $\text{km}$ ) of sprites with a halo. The  
 236 Pearson correlation coefficient ( $r$ ) and the linear fit equation ( $Y$ ,  $\text{km}$ ) are denoted on the top  
 237 corner of each panel. The weak correlations are insignificant and therefore not presented.

### Sprite top altitude



238

239 Fig. 2. Lightning fall-time ( $X$ ,  $\mu\text{s}$ ) (top left row), normalized peak electric field ( $E$ ,  $\text{kV/m}$ ) (top middle row), and  
 240 peak current ( $I$ ,  $\text{kA}$ ) (top right row) versus the top altitude ( $Y$ ,  $\text{km}$ ) of carrot sprites. Lightning rise-time ( $T$ ,  $\mu\text{s}$ )  
 241 (middle left row) and normalized peak electric field ( $E$ ,  $\text{kV/m}$ ) (middle center row) versus the top altitude ( $Y$ ,

242 km) of column sprites. Lightning fall-time ( $X$ ,  $\mu\text{s}$ ) (bottom left row) and peak current ( $I$ , kA) (bottom right row)  
243 versus top altitude ( $Y$ , km) of sprites with a halo. Green, purple, red, yellow, and black dots on the sprite with a  
244 halo plot shows column, carrot, wishbone, jellyfish, and “column and carrot” sprites, respectively. The Pearson  
245 correlation coefficient ( $r$ ) and the linear fit equation ( $Y$ , km) are denoted on the top corner of each panel. The  
246 value in parentheses in the linear fit equation is the uncertainty.

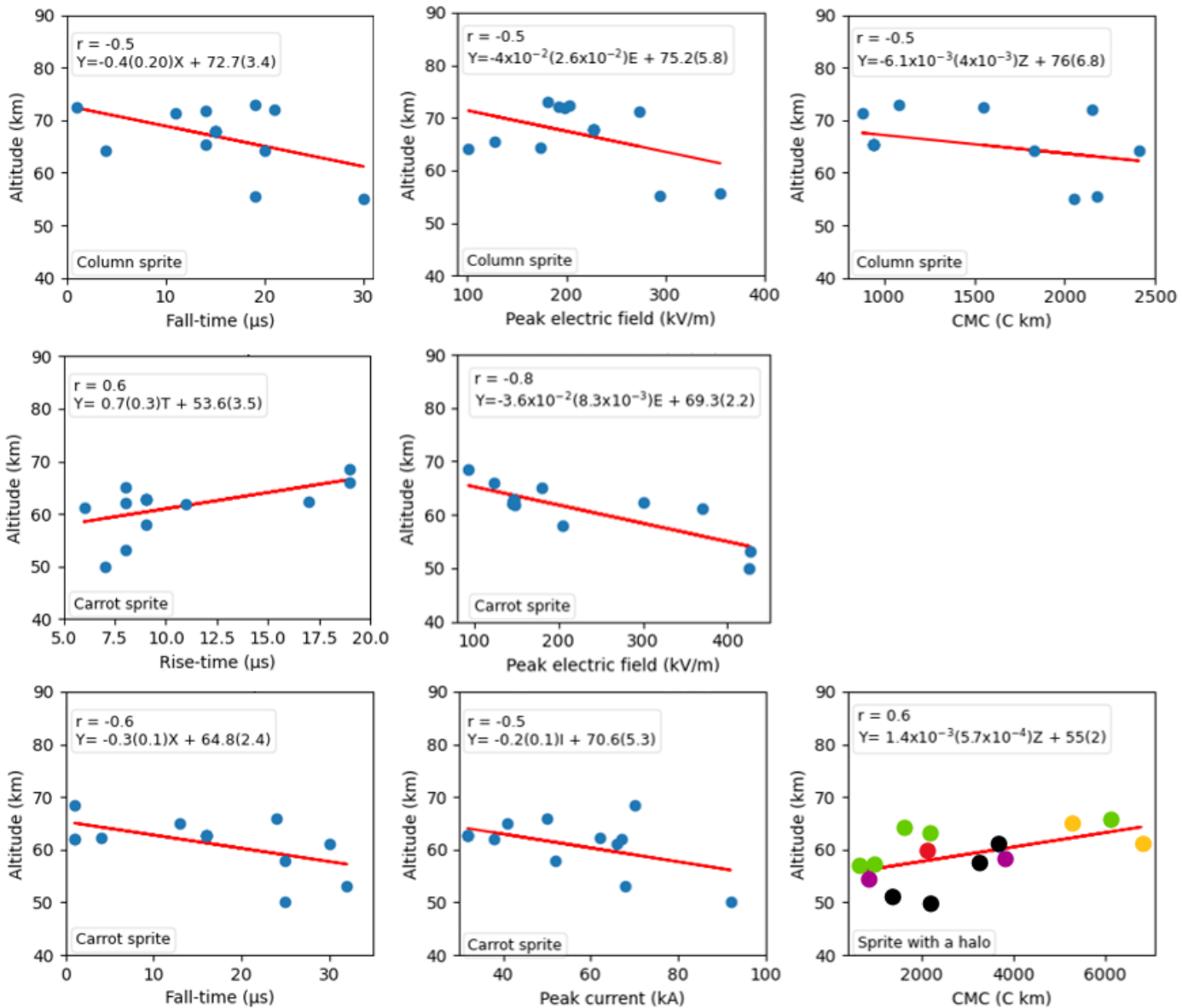
247 The top altitude of column sprites against lightning rise-time and peak electric field showed  
248 good positive and negative linear correlations (0.5) and (-0.6), respectively. The good  
249 positive (0.5) and weak negative (-0.2) (not shown) correlations found between the lightning  
250 rise-time and fall-time against the top altitude of column sprites, respectively, might be  
251 associated with the downward propagation of streamers and the lack of upward propagating  
252 streamers during column sprites initiation processes (Bór, 2013).

253 The top altitude of carrot sprites against lightning fall-time, peak electric field, and peak  
254 current showed good negative linear correlations (-0.6), (-0.7), and (-0.5), respectively. The  
255 top altitude of sprites with halos against lightning fall-time and peak current showed good  
256 positive linear correlations (0.7) and (0.5), respectively. For carrot sprites, this suggests that  
257 the electrical breakdown region decreases in altitude for a longer fall-time, greater peak  
258 electric field, and greater peak current.

### 259 **3.2 Sprites brightest region altitude**

260 Fig. 3 shows the relationship between lightning fall-time ( $X$ ,  $\mu\text{s}$ ) (top left row), normalized  
261 peak electric field ( $E$ , kV/m) (top middle row), and CMC ( $Z$ , C-km) (top right row) versus  
262 the altitude ( $Y$ , km) of the brightest region for column sprites. Fig. 3 also shows lightning  
263 rise-time ( $T$ ,  $\mu\text{s}$ ) (middle left row), normalized peak electric field ( $E$ , kV/m) (middle center  
264 row), fall-time ( $X$ ,  $\mu\text{s}$ ) (bottom left row), and peak current ( $I$ , kA) (bottom center row) versus  
265 the altitude ( $Y$ , km) of the brightest region for carrot sprites (middle row), as well as lightning  
266 CMC ( $Z$ , C-km) (bottom right row) versus the altitude ( $Y$ , km) of the brightest region for  
267 sprites with a halo (bottom row). The Pearson correlation coefficient ( $r$ ) and the linear fit  
268 equation ( $Y$ , km) are denoted on the top corner of each panel.

## Sprite brightest region



269

270 Fig. 3. Lightning fall-time (X,  $\mu\text{s}$ ) (top left row), normalized peak electric field (E, kV/m) (top middle row), and  
 271 CMC (Z, C-km) (top right row) versus the altitude (Y, km) of the brightest region for column sprites. Lightning  
 272 rise-time (T,  $\mu\text{s}$ ) (middle left row), normalized peak electric field (E, kV/m) (middle center row), fall-time (X,  
 273  $\mu\text{s}$ ) (bottom left row), and peak current (I, kA) (bottom center row) versus the altitude (Y, km) of the brightest  
 274 region for carrot sprites (middle and bottom row). Lightning CMC (Z, C-km) (bottom right row) versus the  
 275 altitude (Y, km) of the brightest region for sprites with a halo (bottom right row). Green, purple, red, yellow, and  
 276 black dots on the sprite with a halo plot show column, carrot, wishbone, jellyfish, and “column and carrot”  
 277 sprites, respectively. The Pearson correlation coefficient (r) and the linear fit equation (Y, km) are denoted on  
 278 the top corner of each panel. The value in parentheses in the linear fit equation is the uncertainty.

279 For column sprites, there are good negative correlations for the altitude of maximum  
 280 brightness versus lightning fall-time (-0.5), peak electric field (-0.5), and CMC (-0.5). The

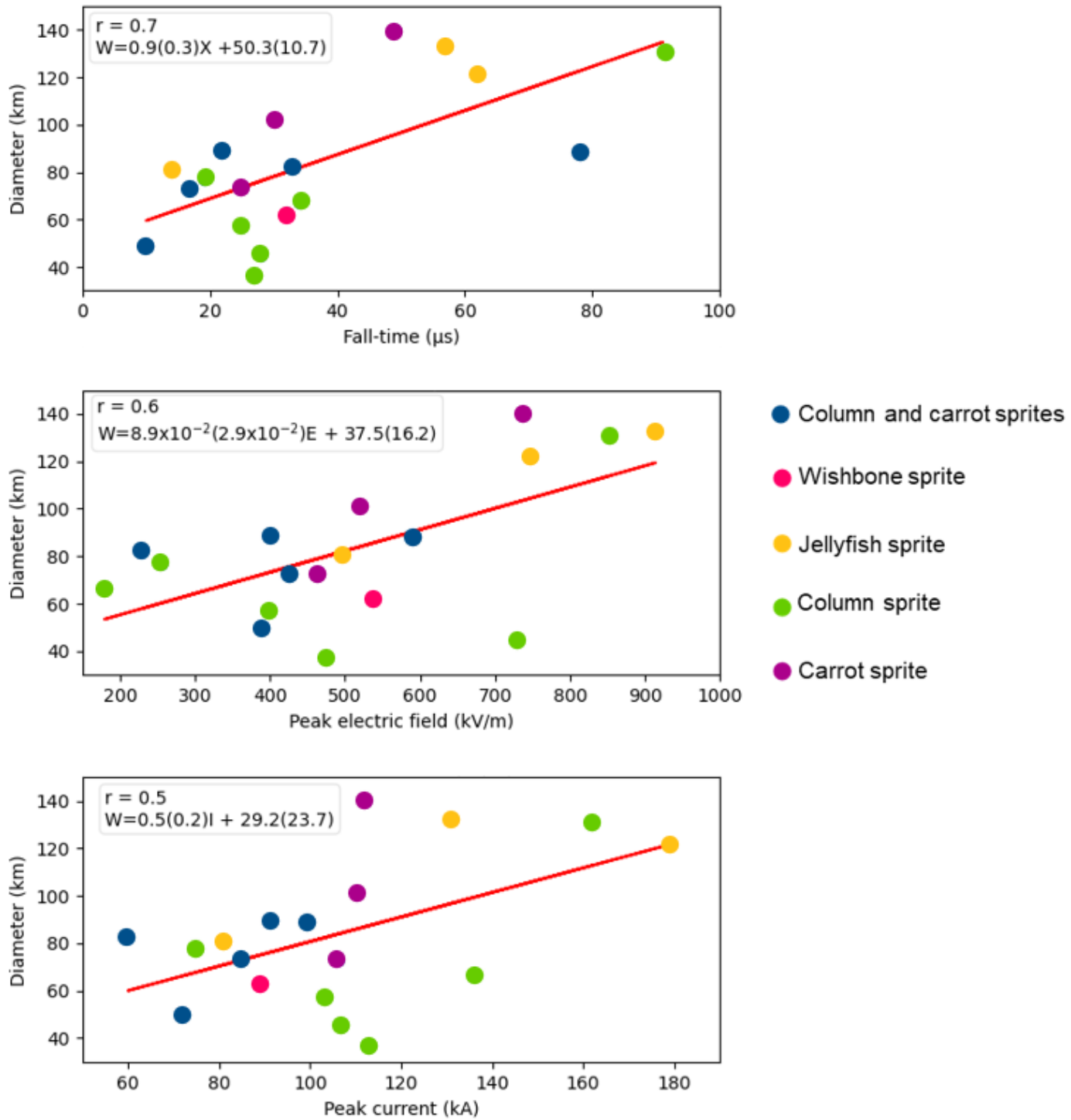
281 altitude of maximum brightness for carrot sprites shows a good positive correlation against  
282 lightning rise-time (0.6) and a good negative correlation against lightning peak electric field  
283 (-0.8), peak current (-0.5), and fall-time (-0.6). The good positive and negative correlation for  
284 carrot sprites against lightning rise-time and fall-time, respectively, might be related to the  
285 downward and upward propagation of streamers during carrot sprites initiation (Bór, 2013).  
286 On the other hand, for any sprites with halos, the altitude of maximum brightness has a good  
287 positive correlation with lightning CMC (0.6).

288 The results indicate that lightning with a longer fall-time, larger electric field, larger peak  
289 current, and larger CMC tend to deposit more energy at lower altitudes for column and carrot  
290 sprites, as shown in Fig. 3. However, lightning with larger CMC tends to deposit more energy  
291 at higher altitudes for sprites with a halo.

### 292 **3.3 Sprites with a halo diameter**

293 Fig. 4 shows the relationship between lightning fall-time ( $X$ ,  $\mu\text{s}$ ) (top panel), normalized peak  
294 electric field ( $E$ ,  $\text{kV/m}$ ) (middle panel), and peak current ( $I$ ,  $\text{kA}$ ) (bottom panel) versus halo  
295 diameters ( $W$ ,  $\text{km}$ ) for different types of sprites. The Pearson correlation coefficient ( $r$ ) and  
296 the linear fit equation ( $W$ ,  $\text{km}$ ) are denoted on the top corner of each panel.

## Sprite with a halo diameter



297

298 Fig. 4. Lightning fall-time ( $X$ ,  $\mu\text{s}$ ) (top panel), normalized peak electric field ( $E$ ,  $\text{kV/m}$ ) (middle panel), and peak  
 299 current ( $I$ ,  $\text{kA}$ ) (bottom panel) versus halo diameters ( $W$ ,  $\text{km}$ ) for different types of sprites (color coded). Note  
 300 that the “column and carrot sprites” are where both types occur together. The Pearson correlation coefficient ( $r$ )  
 301 and the linear fit equation ( $W$ ,  $\text{km}$ ) are denoted on the top corner of each panel. The value in parentheses in the  
 302 linear fit equation is the uncertainty.

303 We found that halo diameters span between 37 and 140 km with an average of 84 (31) km,  
304 where the standard deviation is given in parentheses. A correlation coefficient of 0.7 exists  
305 between lightning fall-time and halo diameter, and a correlation coefficient of 0.6 exists  
306 between normalized lightning peak electric field and halo diameter. The lightning peak  
307 current and halo diameter show a good correlation (0.5), see Fig. 4. In all cases, the larger the  
308 lightning peak electric field, peak current, and fall-time, the larger the halo diameters.

309 A decrease in lightning parameter with altitude follows the behaviour of the electric field and  
310 Maxwellian relaxation time in the Earth's atmosphere (Liu et al., 2015). It is known that the  
311 lightning CMC magnitude also depends on the duration of the continuing current. Thus, a  
312 longer continuing current enhances the lightning CMC magnitude estimate. The results  
313 suggest that the larger lightning CMC and fall-time are capable of sustaining maximum  
314 photon production at a low altitude compared to small lightning CMC and fall-time. The  
315 lightning CMC, peak electric field, peak current, rise-time and fall-time are essential in the  
316 generation and development of TLEs or sprites morphologies.

317 The results show that the lightning rise-time, fall-time, CMC, peak current, and peak electric  
318 field are essential in determining whether the lightning discharge initiated the TLEs or what  
319 type of sprites morphologies were initiated. The lightning rise-time, which is not usually  
320 reported (Asano et al., 2008; Haspel et al., 2020) and lightning fall-time, which has not been  
321 reported in TLEs literature, should be included in the future lightning and TLEs studies.

### 322 **Acknowledgments**

323 DM thanks the South African National Space Agency and the University of KwaZulu-Natal  
324 for funding. DM, KM, and MF work was supported by the Royal Society (UK) grant  
325 NMG/R1/180252. JM acknowledges support from the National Science Centre, Poland,  
326 under grant 2015/19/B/ST10/01055. We thank Nickolay Ivchenko for operating the camera  
327 system from one of our observation sites.

### 328 **Data availability**

329 On request from the author (s)

### 330 **References**

331 Asano, T., Hayakawa, M., Cho, M. and Suzuki, T., 2008. Computer simulations on the  
332 initiation and morphological difference of Japan winter and summer sprites. *J. Geophys. Res.*  
333 *Space Phys*, 113(A2). <https://doi.org/10.1029/2007ja012528>

334 Bering III, E. A., Benbrook, J. R., Bhusal, L., Garrett, J. A., Paredes, A. M., Wescott, E. M.,  
335 ... and Lyons, W. A. 2004. Observations of transient luminous events (TLEs) associated with  
336 negative cloud to ground (– CG) lightning strokes. *Geophys. Res. Lett.* 31(5).  
337 <https://doi.org/10.1029/2003gl018659>

338 Bór, J. 2013. Optically perceptible characteristics of sprites observed in Central Europe in  
339 2007–2009. *J. Atmos. Sol. Terr. Phys.* 92, 151-177.  
340 <https://doi.org/10.1016/j.jastp.2012.10.008>

341 Chen, A.B.C., Chen, H., Chuang, C.W., Cummer, S.A., Lu, G., Fang, H.K., Su, H.T. and  
342 Hsu, R.R., 2019. On negative sprites and the polarity paradox. *Geophys. Res. Lett.* 46(16),  
343 9370-9378. <https://doi.org/10.1029/2019gl083804>

344 Cooray, V. and Lobato, A., 2020. The Energy, Momentum, and Peak Power Radiated by  
345 Negative Lightning Return Strokes. *Atmos.* 11(12), 1288.  
346 <https://doi.org/10.3390/atmos11121288>

347 Earthnetworks.com. (2019). Sferic Maps [online] Available at:  
348 <<https://www.earthnetworks.com/product/decision-support-collaboration-tools/sferic-maps/>>  
349 [Accessed 01 February 2019]

350 Frey, H.U., Mende, S.B., Cummer, S.A., Li, J., Adachi, T., Fukunishi, H., Takahashi, Y.,  
351 Chen, A.B., Hsu, R.R., Su, H.T. and Chang, Y.S., 2007. Halos generated by negative cloud-  
352 to-ground lightning. *Geophys. Res. Lett.* 34(18). <https://doi.org/10.1029/2007gl030908>

353 Füllekrug, M., Mareev, E.A. Rycroft, M.J. eds., 2006. Sprites, Elves and intense Lightning  
354 Discharges (Vol. 225). NATO Science Series II. Mathematics, physics and chemistry,  
355 Dordrecht: Springer, ISBN 1-4020-4628-630-42, 30-32. <https://doi.org/10.1007/1-4020-4629-4>

357 Füllekrug, M., 2010. Wideband digital low-frequency radio receiver. *Meas. Sci. Technol.*  
358 21(1), 1-9. <https://doi.org/10.1088/0957-0233/21/1/015901>

359 Füllekrug, M., Nnadih, S., Soula, S et al., 2019. Maximum sprite streamer luminosity near the  
360 Stratopause. *Geophys. Res. Lett.* 46(21), 12572-12579.  
361 <https://doi.org/10.1029/2019GL084331>

362 Gamerota, W.R., Cummer, S.A., Li, J., Stenbaek-Nielsen, H.C., Haaland, R.K. and McHarg,  
363 M.G., 2011. Comparison of sprite initiation altitudes between observations and models. *J.*  
364 *Geophys. Res. Space. Phys.* 116(A2). <https://doi.org/10.1029/2010ja016095>



365 Gijben, M., 2012. The lightning climatology of South Africa. *S. Afr. J. Sci.*, 108(3), 1-10.  
366 <https://doi.org/10.4102/sajs.v108i3/4.740>

367 Haspel, C., Tzabari, M. and Yair, Y., 2020. The influence of symmetric and non-symmetric  
368 charge configurations on the possibility of sprite inception: Numerical experiments with a 3D  
369 electrostatic model. *J. Atmos. Sol. Terr. Phys.* 202, 105245.  
370 <https://doi.org/10.1016/j.jastp.2020.105245>

371 Li, J., Cummer, S.A., Lyons, W.A. and Nelson, T.E., 2008. Coordinated analysis of delayed  
372 sprites with high-speed images and remote electromagnetic fields. *J. Geophys. Res. Atmos.*  
373 113(D20). <https://doi.org/10.1029/2008JD010008>

374 Liu, N., McHarg, M.G. and Stenbaek-Nielsen, H.C., 2015. High-altitude electrical discharges  
375 associated with thunderstorms and lightning. *J. Atmos. Sol. Terr. Phys.* 136, 98-118.  
376 <https://doi.org/10.1016/j.jastp.2015.05.013>

377 Liu, N., Boggs, L.D. and Cummer, S.A., 2016. Observation-constrained modeling of the  
378 ionospheric impact of negative sprites. *Geophys. Res. Lett.* 43(6), 2365-  
379 2373. <https://doi.org/10.1002/2016gl068256>

380 Luque, A. and Ebert, U., 2009. Emergence of sprite streamers from screening-ionization  
381 waves in the lower ionosphere. *Nat. Geosci.* 2(11), 757-760. <https://doi.org/10.1038/ngeo662>

382 Luque, A., Stenbaek-Nielsen, H.C., McHarg, M.G. and Haaland, R.K., 2016. Sprite beads  
383 and glows arising from the attachment instability in streamer channels. *J. Geophys. Res.*  
384 *Space. Phys.* 121(3), 2431-2449. <https://doi.org/10.1002/2015ja022234>

385 Malagón-Romero, A., Teunissen, J., Stenbaek-Nielsen, H.C., McHarg, M.G., Ebert, U. and  
386 Luque, A., 2020. On the emergence mechanism of carrot sprites. *Geophys. Res. Lett.* 47(1),  
387 e2019GL085776. <https://doi.org/10.1029/2019gl085776>

388 Mashao, D.C., Kosch, M.J., Bór, J et al., 2021. The altitude of sprites observed over South  
389 Africa. *S. Afr. J. Sci.* 117(1-2), 1-8. <https://doi.org/10.17159/sajs.2021/7941>

390 McHarg, M.G., Haaland, R.K., Moudry, D. and Stenbaek-Nielsen, H.C., 2002. Altitude-time  
391 development of sprites. *J. Geophys. Res. Space Phys.* 107(A11), SIA-9.  
392 <https://doi.org/10.1029/2001ja000283>

393 McHarg, M.G., Stenbaek-Nielsen, H.C. and Kammae, T., 2007. Observations of streamer  
394 formation in sprites. *Geophys. Res. Lett.* 34(6), L06804.  
395 <https://doi.org/10.1029/2006GL027854>

396 Miyasato, R., Taylor, M.J., Fukunishi, H. and Stenbaek-Nielsen, H.C., 2002. Statistical  
397 characteristics of sprite halo events using coincident photometric and imaging data. *Geophys.*  
398 *Res. Lett.* 29(21), 29-1. <https://doi.org/10.1029/2001gl014480>

399 Mlynarczyk, J., Bór, J., Kulak, A., Popek, M. and Kubisz, J., 2015. An unusual sequence of  
400 sprites followed by a secondary TLE: An analysis of ELF radio measurements and optical  
401 observations. *J. Geophys. Res. Space Phys.* 120(3), 2241-2254.  
402 <https://doi.org/10.1002/2014ja020780>

403 Mlynarczyk, J., Kulak, A., Klucjasz, S., Martynski, K., Kubisz, J. and Popek, M., 2018, May.  
404 New broadband ELF receiver for studying atmospheric discharges in Central Europe. In *2018*  
405 *Baltic URSI Symposium (URSI)* (pp. 155-157). IEEE.  
406 <https://doi.org/10.23919/ursi.2018.8406729>

407 Nnadih, S., Kosch, M., Martinez, P. and Bor, J., 2018. First ground-based observations of  
408 sprites over southern Africa. *S. A. J. Sci.* 114(9-10), 1-6.  
409 <https://doi.org/10.17159/sajs.2018/4272>

410 Pasko, V.P., Inan, U.S., Bell, T.F. and Taranenko, Y.N., 1997. Sprites produced by quasi-  
411 electrostatic heating and ionization in the lower ionosphere. *J. Geophys. Res. Space.*  
412 *Phys.* 102(A3), 4529-4561. <https://doi.org/10.1029/96ja03528>

413 Pasko, V.P., 2010. Recent advances in theory of transient luminous events. *J. Geophys. Res.*  
414 *Space Phys.* 115(A6). <https://doi.org/10.1029/2009ja014860>

415 Pasko, V.P., Qin, J. and Celestin, S., 2013. Toward better understanding of sprite streamers:  
416 initiation, morphology, and polarity asymmetry. *Surv. Geophys.* 34(6), 797-830.  
417 <https://doi.org/10.1007/s10712-013-9246-y>

418 Peat, J., Barton, B. and Elliott, E., 2009. *Statistics workbook for evidence-based health care.*  
419 John Wiley & Sons, 93-101. <https://doi.org/10.1002/9781444300499>

420 Siingh, D., Singh, R.P., Singh, A.K., Kumar, S., Kulkarni, M.N. and Singh, A.K., 2012.  
421 Discharges in the stratosphere and mesosphere. *Space sci. rev.* 169(1-4), 73-121.  
422 <https://doi.org/10.1007/s11214-012-9906-0>

423 Stenbaek-Nielsen, H.C., Haaland, R., McHarg, M.G., Hensley, B.A. and Kanmae, T., 2010.  
424 Sprite initiation altitude measured by triangulation. *J. Geophys. Res. Space Phys.* 115(A3).  
425 <https://doi.org/10.1029/2009ja014543>

426 Soula, S., van der Velde, O., Montanyà, J., Neubert, T., Chanrion, O. and Ganot, M., 2009.  
427 Analysis of thunderstorm and lightning activity associated with sprites observed during the  
428 EuroSprite campaigns: Two case studies. *Atmos. Res.* 91(2-4), 514-528.  
429 <https://doi.org/10.1016/j.atmosres.2008.06.017>

430 Surkov, V.V. and Hayakawa, M., 2020. Progress in the study of transient luminous and  
431 atmospheric events: a review. *Surv. Geophys.* 41, 1101-1142. [https://doi.org/10.1007/s10712-](https://doi.org/10.1007/s10712-020-09597-2)  
432 020-09597-2

433 Taylor, W.L. and Jean, A.G., 1959. Very-low-frequency radiation spectra of lightning  
434 discharges. *NBS J. Res. Radio Propagation D*, 63(2), 199.  
435 <https://doi.org/10.6028/jres.063d.021>

436 Taylor, M.J., Bailey, M.A., Pautet, P.D et al., 2008. Rare measurements of a sprite with halo  
437 event driven by a negative lightning discharge over Argentina. *Geophys. Res. Lett.* 35(14),  
438 L14812. <https://doi.org/10.1029/2008GL033984>

439 Wescott, E.M., Sentman, D.D., Heavner, M.J et al., 1998. Observations of  
440 'Columniform'sprites. *J. Atmos. Sol. Terr. Phys.* 60(7-9), 733-740.  
441 [https://doi.org/10.1016/s1364-6826\(98\)00029-7](https://doi.org/10.1016/s1364-6826(98)00029-7)

442 Wescott, E.M., Stenbaek-Nielsen, H.C., Sentman, D.D et al., 2001. Triangulation of sprites,  
443 associated halos and their possible relation to causative lightning and micrometeors. *J.*  
444 *Geophys. Res. Space Phys.* 106(A6), 10467-10477. <https://doi.org/10.1029/2000ja000182>

445 Williams, E., Kuo, C.L., Bór, J., Sători, G., Newsome, R., Adachi, T., Boldi, R., Chen, A.,  
446 Downes, E., Hsu, R.R. and Lyons, W., 2012. Resolution of the sprite polarity paradox: The  
447 role of halos. *Radio Sci.* 47(02), 1-12. <https://doi.org/10.1029/2011rs004794>

448 Yang, J., Lu, G., Liu, N., Sato, M., Feng, G., Wang, Y. and Chou, J.K., 2017. Sprite possibly  
449 produced by two distinct positive cloud-to-ground lightning flashes. *TAO: Terr. Atmos.*  
450 *Ocean. Sci.* 28(4), 609-624. <https://doi.org/10.3319/tao.2016.07.22.01>

451 Yaniv, R., Yair, Y., Price, C., Sato, M., Hobara, Y., Cummer, S., Li, J. and Devir, A., 2014.  
452 Ground-based observations of the relations between lightning charge-moment-change and the  
453 physical and optical properties of column sprites. *J. Atmos. Sol. Terr. Phys.* 107, 60-67.  
454 <https://doi.org/10.1016/j.jastp.2013.10.018>

455 Zhu, Y., Rakov, V.A., Tran, M.D et al., 2017. Evaluation of ENTLN performance  
456 characteristics based on the ground truth natural and rocket-triggered lightning data acquired

457 in Florida. *J. Geophys. Res. Atmos.* 122(18), 9858-9866.

458 <https://doi.org/10.1002/2017JD027270>

459

460 **Appendix**

461 Table 1. Summary of column and carrot sprites and sprites with halos including time, date,  
 462 CG lightning strokes position and lightning peak current as reported by SAWS and EN;  
 463 distance from the ELF receiver to the lightning location; lightning electric fields, rise-times,  
 464 and fall-times computed from the ELF data; lightning CMC enumerated from the broadband  
 465 magnetic field recording in the Bieszczady Mountains (49.20° N. 22.54° E), Poland; and  
 466 TLEs estimated top altitude and altitude of the brightest region. Different font color shows  
 467 information related to sprites with halos (purple), column sprites (blue), and carrot sprites  
 468 (black).

Time (UTC)	LAT (°)	LON (°)	Peak current (kA)	Distance from ELF receiver to lightning (km)	Electric Field at 1 km from lightning location (kV/m)	Rise-time (μs)	Fall-time (μs)	CMC (C-km)	TLEs top altitude (km)	TLEs altitude of brightest region (km)	Halo diameter (km)
2019-02-01 18:45:10.752	-29.24	25.35	113	376.8	475.0	10	27	6090	72.7	65.5	37
2019-02-01 19:43:09.728	-29.60	25.07	103	333.4	396.6	11	25	2150	79.5	63.0	57
2019-02-01 20:10:11.537	-28.78	25.86	89	445.9	539.6	12	32	2130	75.6	60.2	63
2019-02-01 20:14:00.121	-29.71	25.29	60	347.3	229.3	8	33	3240	83.3	58.0	82
2019-02-01 20:29:36.130	-28.57	25.14	110	404.9	518.9	11	30	3790	80.5	58.5	102
2019-02-01 21:05:14.339	-29.24	24.62	75	319.1	255.8	22	19	689	82.3	56.6	77
2019-02-01 21:05:14.439	-29.05	24.78	72	344.3	388.8	10	10	3683	72.1	60.7	50
2019-02-01 21:18:40.722	-28.55	25.61	179	441.6	748.9	15	62	5270	86.0	65.0	122
2019-02-01 21:54:07.906	-28.90	26.63	131	504.4	914.0	8	57	6780	85.5	61.3	133
2019-02-02 20:54:36.370	-31.04	27.04	91	483.4	401.6	13	78	1340	79.9	51.4	89
2019-02-02 21:11:55.386	-30.25	26.58	99	448.6	592.4	16	22	2170	76.6	50.0	89
2019-02-02 22:44:38.719	-31.77	27.19	162	502.3	853.4	18	91	930	90.5	57.1	131
2019-02-11 19:53:57.116	-28.24	26.41	112	707.5	737.8	10	49	840	74.6	55.0	140
2019-01-30 20:40:17.642	-29.29	23.65	136	241.9	179.5	9	34	1620	81.2	64.0	67
2019-02-11 19:46:46.836	-28.22	25.66	107	656.1	727.2	8	28		83.3	68.0	45
2019-02-01 20:19:35.061	-29.02	25.34	106	389.1	463.5	10	25		71.5	59.0	73
2019-02-02 22:06:00.242	-31.18	26.98	81	476.7	496.6	25	14		73.6	57.0	81
2019-02-02 21:06:16.417	-30.96	27.19	85	496.4	425.8	14	17		72.0	50.0	73
2019-02-01 19:05:21.584	-29.38	25.21	50	357.3	355.4	10	19	2180	72.4	55.6	
2019-02-02 21:53:21.111	-31.15	27.02	50	481.0	293.6	7	30	2050	76.2	55.1	
2019-01-29 19:39:29.981	-29.42	24.39	34	289.1	100.8	12	20	1830	83.5	64.2	
2019-01-29 20:49:49.668	-29.23	24.79	56	332.7	173.7	16	4	2410	83.3	64.3	

2019-01-29 22:48:06.932	-28.18	24.71	44	406.4	203.1	10	1	1550	82.6	72.4	
2019-01-29 23:03:02.432	-28.13	24.69	34	410.2	192.0	11	21	2150	82.4	72.0	
2019-01-29 23:10:49.261	-27.91	24.32	51	421.3	181.1	10	19	1080	86.0	73.0	
2019-01-30 21:19:28.474	-29.34	24.82	87	328.0	274.3	11	11	880	79.8	71.3	
2019-01-30 22:05:21.758	-28.97	24.73	37	345.8	126.8	7	14	940	76.0	65.4	
2019-01-29 23:00:17.969	-28.20	25.06	36	428.9	197.6	15	14		86.4	71.8	
2019-02-01 19:24:25.922	-29.79	25.20	54	336.1	227.1	13	15		75.9	67.8	
2019-02-01 19:12:42.451	-29.86	25.41	62	351.5	301.0	17	4	2050	78.6	62.3	
2019-02-01 19:26:48.376	-29.56	25.04	41	332.9	179.6	8	13	1930	86.2	65.1	
2019-02-01 20:09:16.344	-29.62	25.20	66	344.2	369.6	6	30	3045	78.4	61.2	
2019-02-01 20:38:25.718	-28.61	25.53	68	431.1	427.4	8	32	2200	79.3	53.1	
2019-01-29 19:33:50.302	-29.40	24.33	50	285.2	124.0	19	24	1360	83.7	66.0	
2019-01-29 20:25:41.984	-29.51	25.18	38	347.6	144.7	8	1	3060	85.0	62.0	
2019-01-29 20:38:40.528	-29.45	25.18	67	350.6	148.2	11	1	2160	87.0	62.0	
2019-01-29 19:17:59.218	-30.13	24.35	70	245.9	93.3	19	1	1680	83.3	68.5	
2019-02-01 19:55:34.857	-29.35	25.44	52	378.3	204.7	9	25		74.1	57.9	
2019-02-01 20:15:43.526	-29.02	25.32	92	387.6	425.3	7	25		70.7	50.0	
2019-02-01 19:24:26.151	-30.05	24.90	32	297.8	146.4	9	16		80.8	62.7	

469